

Article

# Prediction of Optical and Non-Optical Water Quality Parameters in Oligotrophic and Eutrophic Aquatic Systems Using a Small Unmanned Aerial System

Juan G. Arango \* and Robert W. Nairn 

The Center for Restoration of Ecosystems and Watershed, School of Civil Engineering and Environmental Science, University of Oklahoma, Norman, OK 73019, USA; nairn@ou.edu

\* Correspondence: juan.g.arango@ou.edu

Received: 12 November 2019; Accepted: 21 December 2019; Published: 24 December 2019



**Abstract:** The purpose of this study was to create different statistically reliable predictive algorithms for trophic state or water quality for optical (total suspended solids (TSS), Secchi disk depth (SDD), and chlorophyll-a (Chl-a)) and non-optical (total phosphorus (TP) and total nitrogen (TN)) water quality variables or indicators in an oligotrophic system (Grand River Dam Authority (GRDA) Duck Creek Nursery Ponds) and a eutrophic system (City of Commerce, Oklahoma, Wastewater Lagoons) using remote sensing images from a small unmanned aerial system (sUAS) equipped with a multispectral imaging sensor. To develop these algorithms, two sets of data were acquired: (1) In-situ water quality measurements and (2) the spectral reflectance values from sUAS imagery. Reflectance values for each band were extracted under three scenarios: (1) Value to point extraction, (2) average value extraction around the stations, and (3) point extraction using kriged surfaces. Results indicate that multiple variable linear regression models in the visible portion of the electromagnetic spectrum best describe the relationship between TSS ( $R^2 = 0.99$ ,  $p$ -value =  $<0.01$ ), SDD ( $R^2 = 0.88$ ,  $p$ -value =  $<0.01$ ), Chl-a ( $R^2 = 0.85$ ,  $p$ -value =  $<0.01$ ), TP ( $R^2 = 0.98$ ,  $p$ -value =  $<0.01$ ) and TN ( $R^2 = 0.98$ ,  $p$ -value =  $<0.01$ ). In addition, this study concluded that ordinary kriging does not improve the fit between the different water quality parameters and reflectance values.

**Keywords:** remote sensing; small unmanned aerial system; water quality; optical and non-optical water quality parameters

## 1. Introduction

The United States Geological Survey (USGS), in their National Water Quality Assessment Program (NAWQA), defines water quality monitoring as a continuous period of data collection (in lakes, streams, rivers, reservoirs, wetlands, or oceans), in order to evaluate the chemical, physical, and biological characteristics of the body of water with respect to its ecological conditions and designated water uses [1]. Monitoring water quality typically involves a series of in-situ observations, measurements, and water sample collections that are analyzed for various parameters depending on the individual project goals, such as temperature, phosphorus (P), nitrogen (N), total solids, pH, fecal bacteria, conductivity, dissolved oxygen (DO), biochemical oxygen demand (BOD), hardness, alkalinity, suspended sediments, other nutrients, trace metals, and water clarity. Traditionally, water quality indicators are determined by the collection, field examination, and laboratory analyses of water samples, following consistent protocols and guidelines [2].

Although properly collected and analyzed in-situ measurements are highly accurate, these measurements can be time-consuming, susceptible to errors (especially visual subjectivity), and can only be related to a specific point in time and space [3,4]. Due to these potential problems, water quality

monitoring programs that rely solely on these types of measurements may fail to provide accurate spatial or temporal views of water quality.

Considering the above constraints, the use of remote sensing and satellite imagery in water quality monitoring and management has been widely implemented to estimate different water quality parameters [5–7]. Images from different Earth observing satellites (e.g., Landsat 5, Landsat 7, Landsat 8, Terra, Aqua, SPOT, among others) with the capability of obtaining information in the visible (0.4–0.8  $\mu\text{m}$ ), near infrared (0.8–1  $\mu\text{m}$ ) (NIR), and thermal (10–12  $\mu\text{m}$ ) portions of the electromagnetic (EM) spectrum, have been used to estimate different water quality parameters, such as total suspended solids (TSS), chlorophyll-a (Chl-a), pH, colored dissolved organic matter (CDOM), and Secchi disk depth (SDD). In case 1 waters (i.e., oceans), determination of optical properties is affected by phytoplankton. In case 2 waters (i.e., inland waters), determination of optical properties is more complex, due to the presence of dissolved mineral sediments and organic matter [5,6,8–19].

Satellite technology has proven not only to be able to obtain unbiased information on specific characteristics of lakes, but to also serve as a cost-effective complement to in-situ monitoring programs [3]. The implementation of remote sensing and satellite imagery addresses two of the most important limiting factors when obtaining in-situ measurements: (1) The subjective error susceptibility associated with these types of measurements and (2) the limited, discrete sampling point coverage limitation [12].

Despite the benefits of using this technology, a major challenge when using optical imagery in observing and determining water quality parameters is its excessive susceptibility to data limitations due to cloud coverage [2,6,20–22]. At the same time, most applications have focused on detection, determination, and prediction of optical water quality parameters like Chl-a, SDD, and CDOM [21,23–26].

However, in recent years, the collection of high-resolution images using small unmanned aerial systems (sUAS) has become more prevalent [27–31]. Pairing sUAS with multispectral sensors may provide cloud free images with higher revisiting time (temporal resolution) and smaller spatial resolutions at relatively low costs [32,33]. Particularly, for water quality monitoring and modeling, different authors have developed site specific models using multispectral images collected with sUAS [34,35]. Su and Chou [34] used a multispectral sensor onboard an sUAS in order to map the trophic state of Tain-Pu reservoir in Kinmen, Taiwan. As part of their findings, they determined that the ratio between multispectral bands has the ability to predict Chl-a, total phosphorous (TP), and SDD. At the same time, they corroborated that with the flexibility that sUAS offers not only in terms of temporal resolution; but also with respect to higher spatial resolution, stronger regression models can be obtained. Kageyama et al. [35] used an sUAS in order to perform water quality analysis in the Miharu reservoir in Japan. Their findings indicate that the ratios between multispectral bands are helpful to determine chemical oxygen demand (COD), TSS and Chl-a concentrations.

The main purpose of this study was to develop algorithms capable of estimating optical (TSS, Chl-a, SDD) and non-optical (TP and total nitrogen (TN)) water quality parameters in an oligotrophic system and a eutrophic system using images collected with a multispectral sensor attached to an sUAS. Given the global economic and water security challenges posed by increasing nutrient over enrichment and resulting water quality degradation [36–39], systems representing end members of the biological productivity spectrum were selected to generate robust and widely applicable models. Additionally, this study evaluates whether using a well-accepted statistical interpolation method improves the algorithms between the different water quality parameters and the reflectance values.

## 2. Materials and Methods

### 2.1. Study Areas

The area of research for this project involved two human-made pond systems, located on two opposite ends of the biological productivity spectrum. One is an oligotrophic system, while the other one is a eutrophic system (Figure 1).

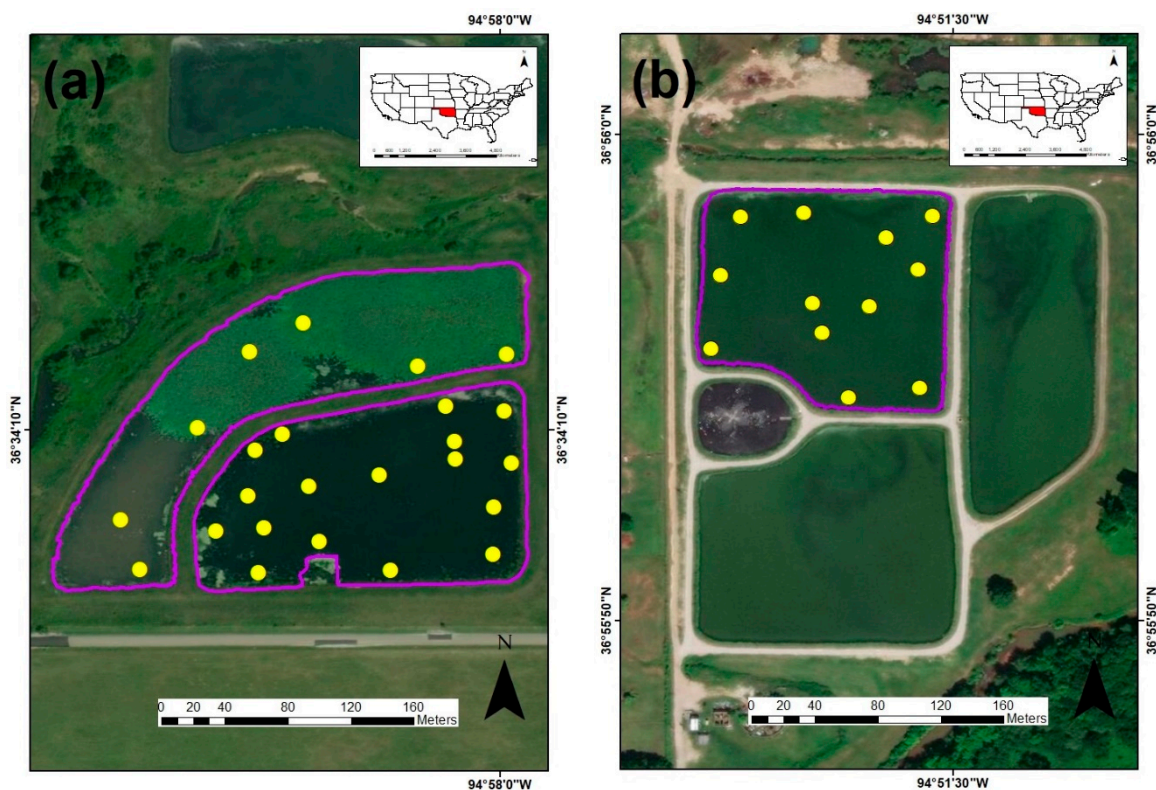


**Figure 1.** Location of the eutrophic and oligotrophic system and sampling stations at each system (yellow dots). (a) Nursery pond, Ottawa County, Oklahoma. (b) Wastewater Lagoons, City of Commerce, Ottawa County, Oklahoma.

The oligotrophic system (the Duck Creek Nursery ponds) were developed as an aquatic plant nursery and receive runoff from surrounding grasslands. The site is located in northeast Oklahoma ( $36.5691^{\circ}$  N,  $-94.9676^{\circ}$  W) (Figure 1a). The nursery ponds (NP) are a series of small ponds, ranging in surface area, located at the upstream part of the Duck Creek arm of Grand Lake O' the Cherokees (Grand Lake). Situated in a watershed of pasture/hay land use, yearly temperatures in the region range from  $-4^{\circ}$  C (in winter) to  $33^{\circ}$  C (in summer) and yearly precipitation ranges from 4.78 cm (in winter) to 13.77 cm (in fall) [40]. The land is owned and managed by the Grand River Dam Authority (GRDA). These ponds are not hydrologically connected to Grand Lake, and are mainly recharged by surface run-off; however, when the water is excessively high in the reservoir (Grand Lake) these ponds serve a flood control function. Two adjacent ponds were included in this study.

The eutrophic system (the City of Commerce Wastewater Lagoons) is located in Commerce, Oklahoma ( $36.9334^{\circ}$  N and  $-94.8730^{\circ}$  W) (Figure 1b). The wastewater lagoons (CL) were reconstructed by the city of Commerce in 2014 and their purpose is to provide primary treatment for the city's municipal wastewater. The primary input of untreated wastewater to these lagoons has excess nitrogen (N), phosphorous (P), and carbon. Domestic wastewater from Commerce enters the system via a clarifier. After a hydraulic retention time (HRT) of 24 h, the clarifier effluent splits into two flow paths. One half of the wastewater goes to the north wastewater lagoon, while the other half goes to the south wastewater lagoon. At each lagoon, wastewater is exposed to sunlight for a period of 3–4 days. The exposure to sunlight contributes to the growth of algae, and the algae builds biomass in order to promote bacteria growth. These bacteria break down the waste present in the water [41]. After adequate HRT, both lagoons discharge their effluent into a third wastewater lagoon that serves as an environmental buffer before discharging the treated effluent to the nearest tributary located at the north-east part of the parcel, in the Grand Lake watershed. Due to its proximity to the Nursery

Ponds (which are approximately 40 km south southwest), yearly temperatures and precipitation are similar. The north lagoon was included in this study.

## 2.2. Water Quality and Multispectral Imagery Data Collection

In total, 36 water samples were collected (24 at the Nursery Ponds and 12 at the Wastewater Lagoons) (Figure 1). At each sampling location, a Secchi Disk Depth (SDD) reading was taken using a 30-cm Secchi Disk attached to a measuring tape. Once completed, one water sample was collected using a 4.2-L PVC depth-discrete horizontal water sampler submerged 0.5 m from the water's surface. Before sample collection, the sampler was rinsed three times with sample water. Once collected, water was divided into four portions. A first portion was transferred to a 250-mL high-density polyethylene (HDPE) bottle for field analyses (turbidity). A second portion was transferred to another 250-mL HDPE bottle to be analyzed for total nitrogen (TN) and total phosphorus (TP). A third portion was transferred to a 1-L dark bottle to be analyzed for chlorophyll-a (Chl-a). Finally, the remaining portion of the sample was transferred to a 1-L bottle to be analyzed for total suspended solids (TSS). Once samples were generated, they were placed into a cooler with ice at 4 °C for later analysis. A properly calibrated YSI 600 multiparameter data sonde [42] was then deployed to obtain dissolved oxygen (DO), temperature, specific conductance, salinity, and pH data. Calibration checks were performed using pH 7 buffer, 1000  $\mu\text{S}/\text{cm}$  conductivity solution, and water saturated air (for DO) during and after sample collection. All samples were collected and preserved according to procedures from the U.S. Environmental Protection Agency (EPA, Washington, DC, USA) [43].

Multispectral imagery was collected using an ATI AgBot sUAS (Aerial Technology International, Oregon City, OR, USA) (Figure 2a) equipped with a MicaSense RedEdge multispectral sensor (MicaSense Inc., Seattle, WA, USA) (Figure 2b), capable of obtaining information in the blue (0.475  $\mu\text{m}$ ), green (0.560  $\mu\text{m}$ ), red (0.668  $\mu\text{m}$ ), red edge (0.717  $\mu\text{m}$ ), and NIR (0.840  $\mu\text{m}$ ) portions of the spectrum. The ATI AgBot is a vertical takeoff and landing (VTOL) carbon fiber frame four-rotor quadcopter (Tri-prop and 4012 400 Kv motors). Onboard, the ATI AgBot carries two dual 6S 6500 mAh lithium polymer (LiPo) battery packs (Pulse Battery, Middletown, IN, USA) (that allow for 26+ minutes of flight time), UBlox GPS, compass module, a downwelling light sensor (DLS) and a MicaSense RedEdge multispectral sensor. The MicaSense RedEdge multispectral sensor is an analog frame camera that has a ground sample distance of 8 cm per pixel (per band) at 120 m above ground level (AGL), a capture rate of 1 capture per second (in all bands), a 16-bit radiometric resolution, and a 47.2° horizontal field of view (HFOV). The sUAS lacks a sun irradiance sensor; however, incident light gets measure by the DLS. This information was supplemented with pre and post photographs (taken with the MicaSense sensor) of MicaSense's calibration reflectance panels in order to improve reflectance in situations where light conditions change during the flight. Including the sensor and batteries, the entire setup weighs 4.7 kg [44].



**Figure 2.** Small unnamed aerial system used to collect multispectral data (a) and MicaSense RedEdge multispectral sensor (b).

To georeference the multispectral images taken with the RedEdge sensor, information from the GPS was transferred to the images via the UBX binary protocol using the NAV and RXM data classes [40]. Differential GPS (DGPS) was obtained using Mission Planner 1.3.68 [45]. No ground control points (GCPs) were defined before the mission (because the mission was flown over water); however, the inertial navigation system (INS) onboard the sUAS provided continuous position, orientation, and velocity of the aircraft. All of this information was transmitted to a ground control station using Mission Planner 1.3.68. Two multiple-waypoint missions were designed in Mission Planner 1.3.68. All missions were flown at an altitude of 100 m with a flying speed of 5 m/s, and estimated flight time of 10 min. For the Nursery Ponds, a total of 164 images with a ground resolution of 6.20 cm were obtained. For the Wastewater Lagoons, a total of 46 images with a ground resolution of 6.20 cm were obtained. Figure 3a,b presents the flight paths for imagery collection at the Nursery Ponds and Wastewater Lagoons, respectively. Multispectral imagery was acquired the same day as the in-situ water samples.



**Figure 3.** Small unmanned aerial system (sUAS) flight path (yellow arrow) and imagery footprint (with number of overlapping pictures) at the Nursery Ponds (a) and Wastewater Lagoon (b).

### 2.3. Methodology

The workflow for this study was divided in four phases: (1) Data collection, (2) data processing, (3) model development, and (4) validation (Figure 4).

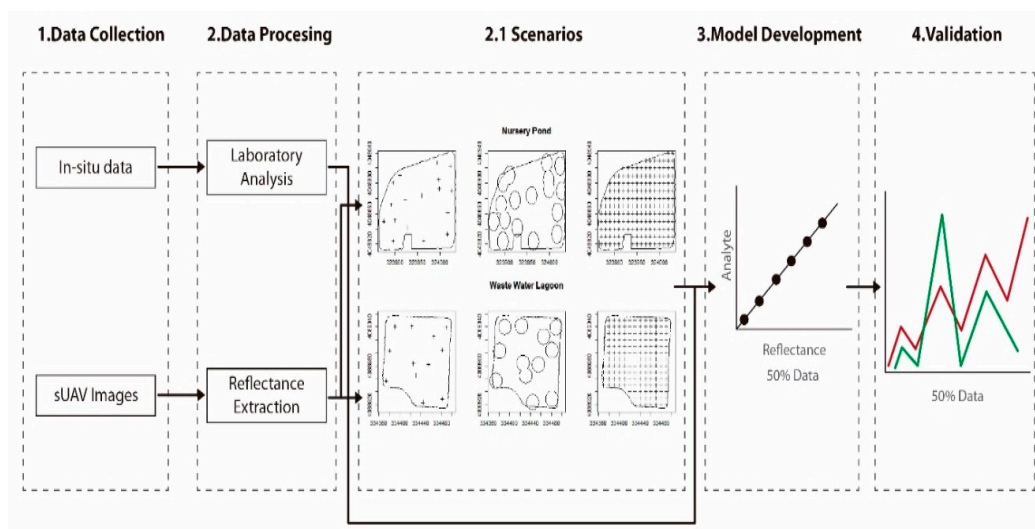


**Figure 4.** Overview of created methodology for the development to statistical water quality models for optical and non-optical water quality parameters.

### 2.3.1. Data Collection

For the Nursery Ponds, in-situ water quality and multispectral imagery collection took place on 12 July 2017, beginning at 11:00 A.M. CST. For the Wastewater Lagoons, in-situ water quality and multispectral imagery collection took place on 8 September 2017, beginning at 2:00 P.M. CST. Multispectral imagery was acquired the same day as the in-situ water samples. Table 1 presents the time window between multispectral data collection and water sample acquisition, using the ending time of the sUAS missions as the reference point.

**Table 1.** Time window between multispectral imagery collection and water samples acquisition for the eutrophic and oligotrophic systems. NP refers to Nursery Pond and CL refers to Wastewater Lagoons.

Nursery Ponds				Wastewater Lagoons	
Site ID	Window (Minutes)	Site ID	Window (Minutes)	Site ID	Window (Minutes)
NP-1	+17	NP-13	+151	CL-1	+22
NP-3	+33	NP-14	+154	CL-2	+38
NP-4	+46	NP-15	+161	CL-3	+47
NP-5	+58	NP-16	+198	CL-4	+57
NP-6	+67	NP-17	+210	CL-5	+68
NP-7	+78	NP-18	+216	CL-6	+79
NP-2	+86	NP-19	+226	CL-7	+86
NP-8	+101	NP-20	+347	CL-8	+97
NP-9	+111	NP-21	+360	CL-9	+108
NP-10	+121	NP-22	+370	CL-10	+114
NP-11	+131	NP-23	+379	CL-11	+125
NP-12	+144	NP-24	+389	CL-12	+130

### 2.3.2. Data Processing

#### Laboratory Analysis

After collection, all water samples were analyzed for TSS, Chl-a, TP, and TN following the methods presented in Table 2. Chl-a samples were filtered through individual glass fiber filters in order to perform pigmentation extraction using 90% acetone, then Chl-a concentrations were measured using a Trilogy laboratory fluorometer at 460 nm. TP samples were individually mixed with a solution of 5N sulfuric acid ( $H_2SO_4$ ), antimony potassium tartrate ( $C_8H_{10}K_2O_{15}Sb_2$ ), ammonium molybdate ( $(NH_4)_2MoO_4$ ), and 0.1M ascorbic acid ( $C_6H_8O_6$ ), and TP concentrations were measured using a Cole Parmer 2800 UV VIS spectrophotometer at 650nm. TN samples were individually mixed with a solution of 3N sodium hydroxide (NaOH), potassium persulfate ( $K_2S_2O_8$ ), nicotinic acid p-toluenesulfonate ( $C_{13}H_{13}NO_5S$ ), and adenosine triphosphate ( $C_{10}H_{16}N_5O_{13}P_3$ ), and TN concentrations were measured with a Lachat Quikchem 8500 series 2 flow injection analysis system. Finally, TSS samples were filtered through individual glass fiber filters (Gelman type A/E), then dried at 105 °C for at least one hour. TSS concentrations were determined by mass difference for the volume of filtered sample.

**Table 2.** Water quality analytes and methods.

Analyte	Method
Chlorophyll $\alpha$	EPA 445.0
Total Phosphorus	SM 4500-P J
Total Nitrogen	SM 4500-P J
Total Suspended Solids	EPA 160.2

#### Reflectance Extraction

In order to perform the extraction of the reflectance values from the multispectral imagery, three scenarios were conducted (Figure 5): (1) Value to point extraction (Figure 5a), where the georeferenced

position of each sampling station was used in order to extract the reflectance; (2) average buffer value extraction (Figure 5b), where a buffer zone of 3 m was created around the georeferenced position of each sampling station in order to extract the average reflectance (the distance of this buffer zone was defined based on the offset distance of the GPS units); and (3) kriging extraction (Figure 5c), where kriged surfaces (using ordinary kriging) were developed for each of the analytes in order to extract the reflectance values of 319 points (oligotrophic system) and 162 points (eutrophic system) inside each created surface. This last scenario was created in order to simulate a hypothetical situation where water samples could be collected from the entire surface of the systems and to determine if the “collection” of more samples (represented by the centroids of each pixel inside the systems) could improve the predictive capability of the models. Ordinary kriging was selected as the interpolation statistical method because concentration estimations (for the different water quality parameters) were to be determined at unsampled locations with minimal error. All imagery stitching and preprocessing were performed in PiX4Dmapper 4.4.9 [46], while the reflectance extractions were performed using ArcMap 10.6 [47].

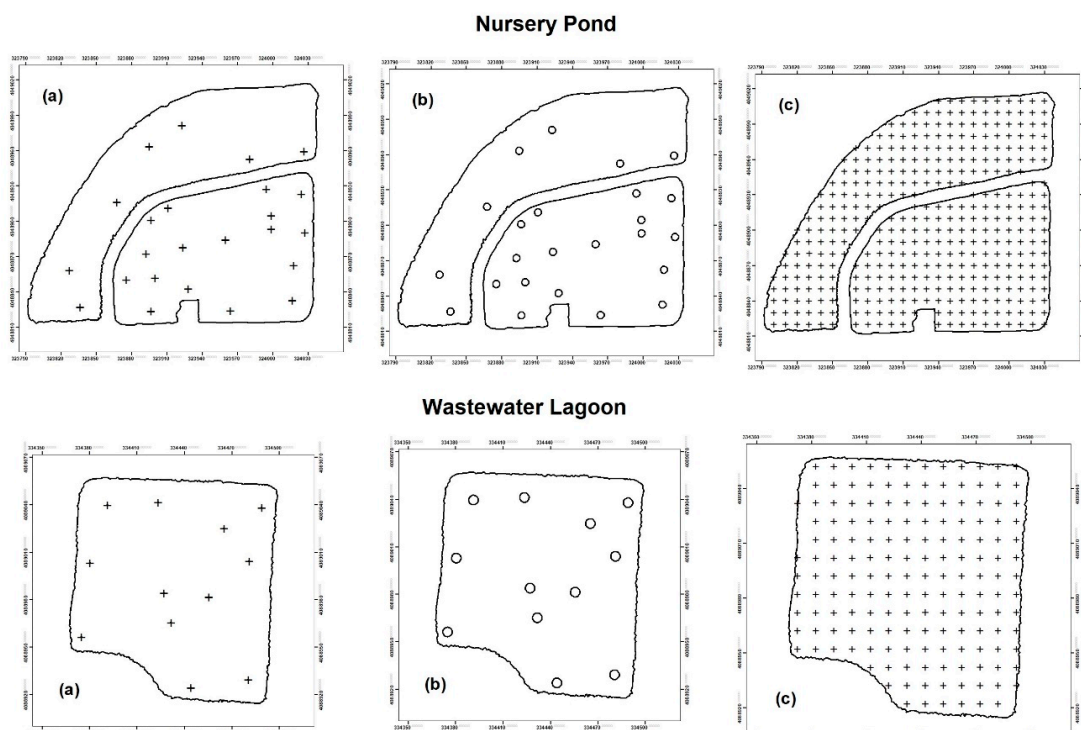


**Figure 5.** Evaluated reflectance extraction scenarios: Point extraction (a), buffer extraction (b), and kriging extraction (c).

### 2.3.3. Model Development and Validation

To ensure equal spatial distribution between both systems, the overall data generated in each system were randomly divided into two subsets. Each subset was then merged with its counterpart. As a result, 50% of the data were used for model development, while the other half was used for model validation.

The models were developed using single variable and multiple variable linear model regression approaches. The untransformed data from in-situ TSS, Chl-a, SDD, TP, and TN values were used as the dependent variables, while the untransformed reflectance of each band, and different ratios between them, were used as the independent variables. The best fit was determined using the coefficient of determination ( $R^2$ ) and the small sample corrected Akaike information criterion (AICc) [48,49]. Once the best fit for each analyte was determined, the remaining 50% of the data were used for validation. Statistical difference was determined using a paired sample *t*-test ( $p$ -value > 0.05) given the

normal distribution of the entire dataset (Shapiro–Wilk test [50]  $p$ -value > 0.05). All statistical analyses were conducted in R 3.5.1 [51].

### 3. Results

#### 3.1. Water Quality

Two systems located at the opposite sides of the biological productivity spectrum were selected for this study. Figures 6 and 7 present the water quality results for the oligotrophic and eutrophic systems, respectively.

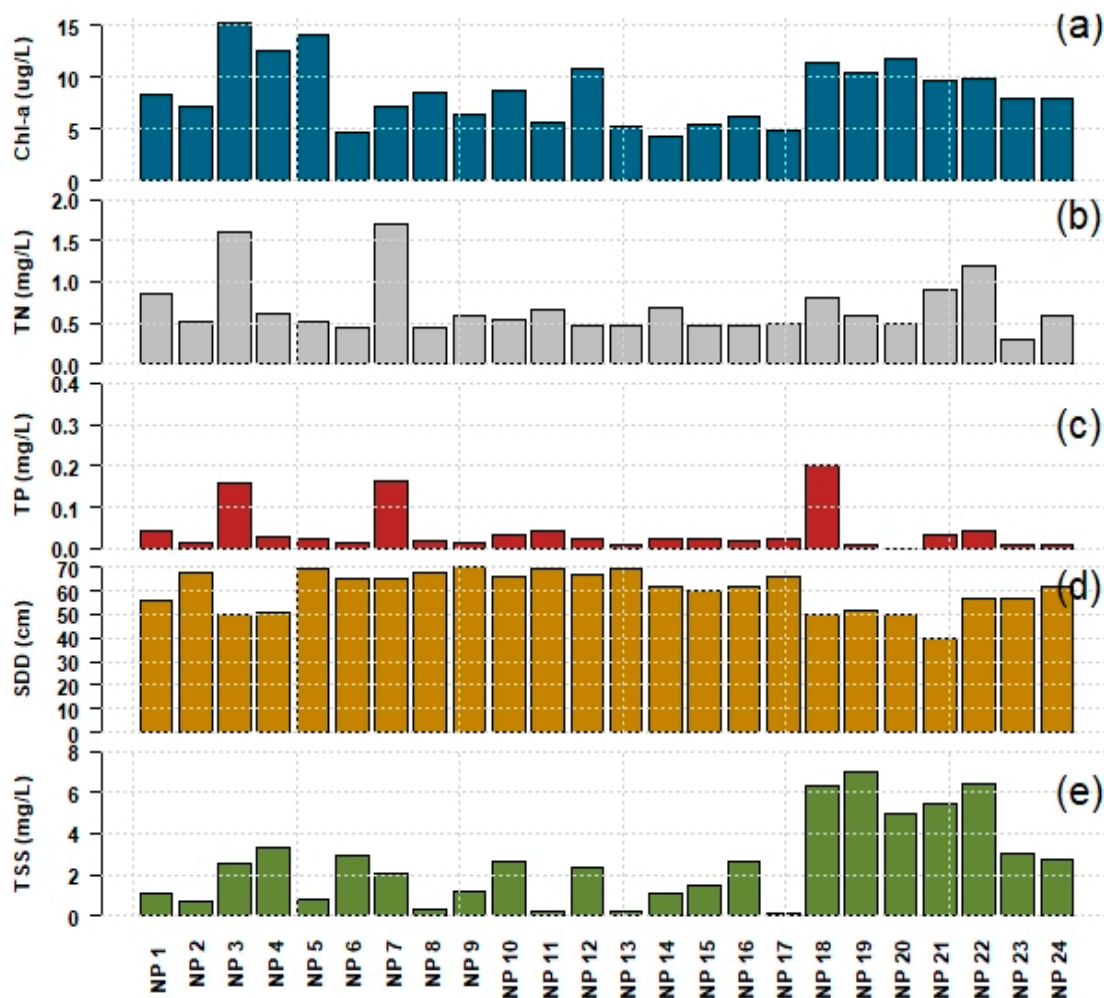


**Figure 6.** Water quality results for the Nursery Ponds (NP) (oligotrophic system). (a) Chlorophyll-a, (b) total nitrogen, (c) total phosphorous, (d) Secchi disk depth, and (e) total suspended solids.

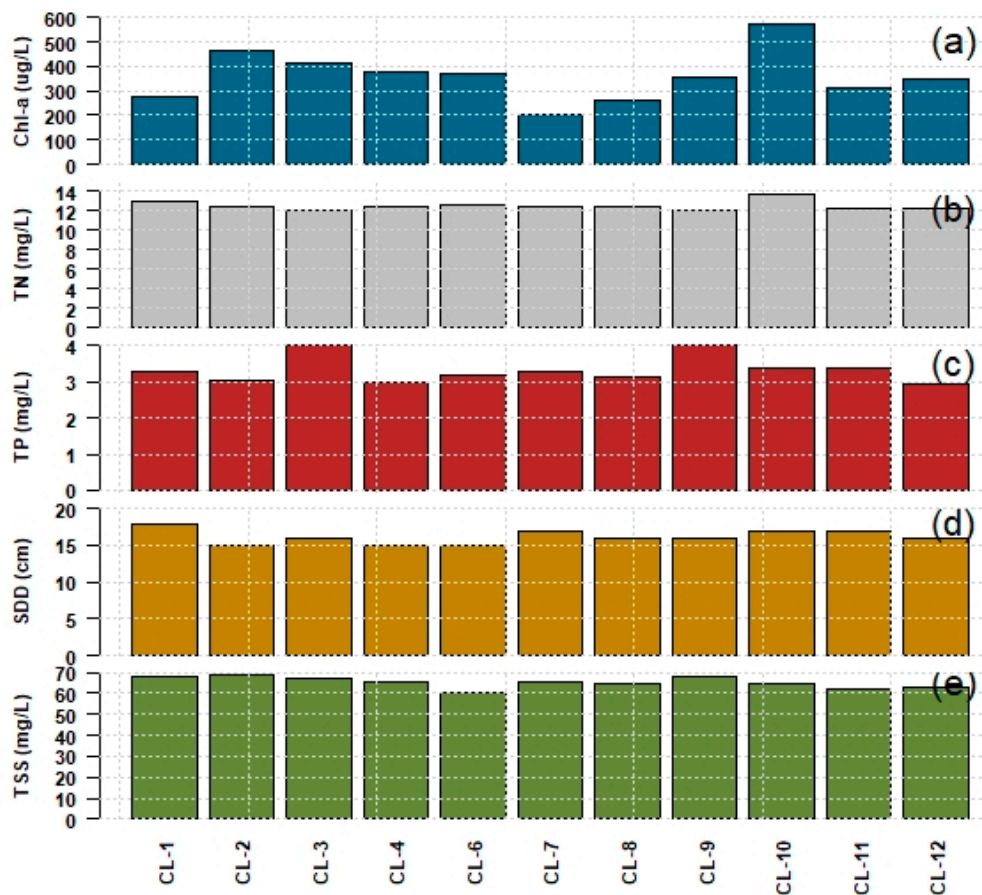


**Figure 7.** Water quality results for the Wastewater Lagoons (CL) (eutrophic system). (a) Chlorophyll-a, (b) total nitrogen, (c) total phosphorous, (d) Secchi disk depth, and (e) total suspended solids.

For the analyzed water quality parameters, substantial differences can be observed between the two systems. Table 3 shows the statistical summary (and comparisons) between the water quality parameters measured at the oligotrophic and eutrophic systems.

**Table 3.** Descriptive statistics and comparison between water quality parameters at the oligotrophic and eutrophic systems. SD refers to standard deviation. Units are  $\mu\text{g/L}$  for Chl-a,  $\text{mg/L}$  for TN, TP and TSS, and  $\text{cm}$  for SDD.

	Oligotrophic System					Eutrophic System				
	Mean	Median	SD	Min	Max	Mean	Median	SD	Min	Max
Chl-a	8.52	8.10	3.08	4.26	15.37	358.3	352.60	103.36	200.40	575.80
TN	0.68	0.56	0.35	0.30	1.71	12.47	12.40	0.47	12.00	13.60
TP	0.04	0.02	0.05	0.01	0.20	3.33	3.27	0.37	2.94	4.02
SDD	60.4	62.00	8.18	40.00	70.00	16.18	16.00	0.98	15.00	18.00
TSS	2.44	2.57	2.09	0.11	7.00	65.33	65.20	2.7	60.20	68.83

### 3.2. Reflectance Extraction

Three scenarios were evaluated under the reflectance extraction procedures: (1) Point extraction, (2) buffer extraction, and (3) Kriging extraction. Figures 8 and 9 present the reflectance values of the oligotrophic and eutrophic systems as a function of the individual stations evaluated in each scenario.

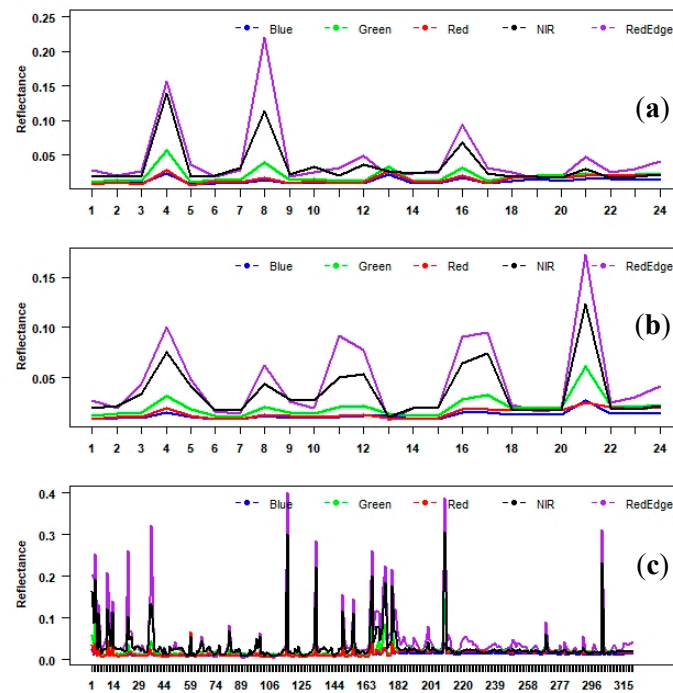


**Figure 8.** Reflectance values (*y*-axis) as a function of the number of stations (*x*-axis) evaluated in the reflectance extraction scenarios. (a) Point extraction, (b) buffer extraction, and (c) Kriging extraction for the oligotrophic system.

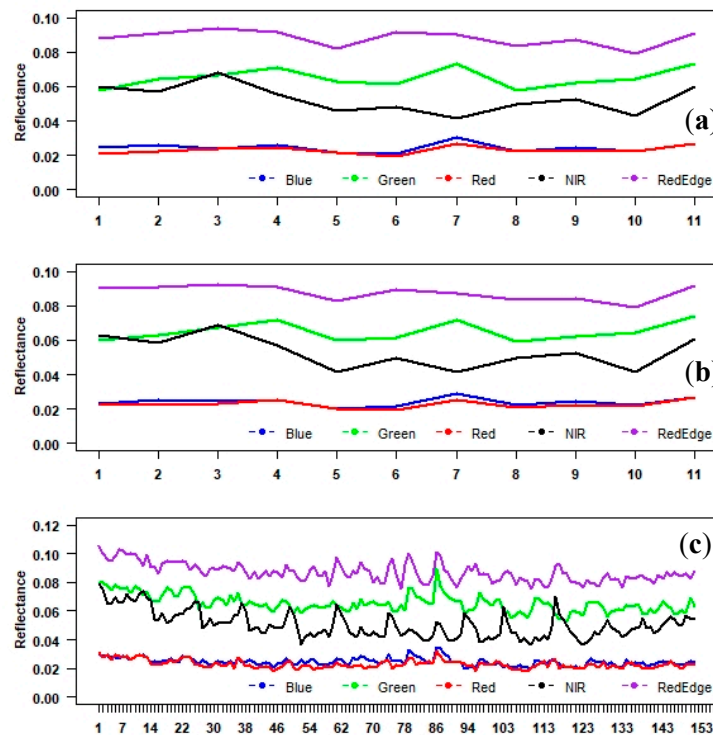


**Figure 9.** Reflectance values (*y*-axis) as a function of the number of stations (*x*-axis) evaluated in the reflectance extraction scenarios. (a) Point extraction, (b) buffer extraction, and (c) Kriging extraction for the eutrophic system.

From the reflectance values as a function of sampling stations, it can be observed that each system provides different relationships, indicating distinct compositions and characteristics. In the oligotrophic system, light reflects more than in the eutrophic system indicating clearer waters.

### 3.3. Models Development and Extraction Scenarios Evaluation

Using a single variable linear model regression approach, a total of 315 models (single bands and band ratios) were developed under the three extraction scenarios (105 models per extraction scenario). For this purpose, the independent variable was defined as the reflectance values from the different bands available from the multispectral sensor and the dependent variable was the in-situ measurements for the different water quality parameters. Considering the predictive capabilities of each model (under each evaluated scenario), it was determined that the point extraction scenario had stronger predictive capabilities (maximum  $R^2$  and minimum AICc values) for all the analyzed parameters (Figure 10).

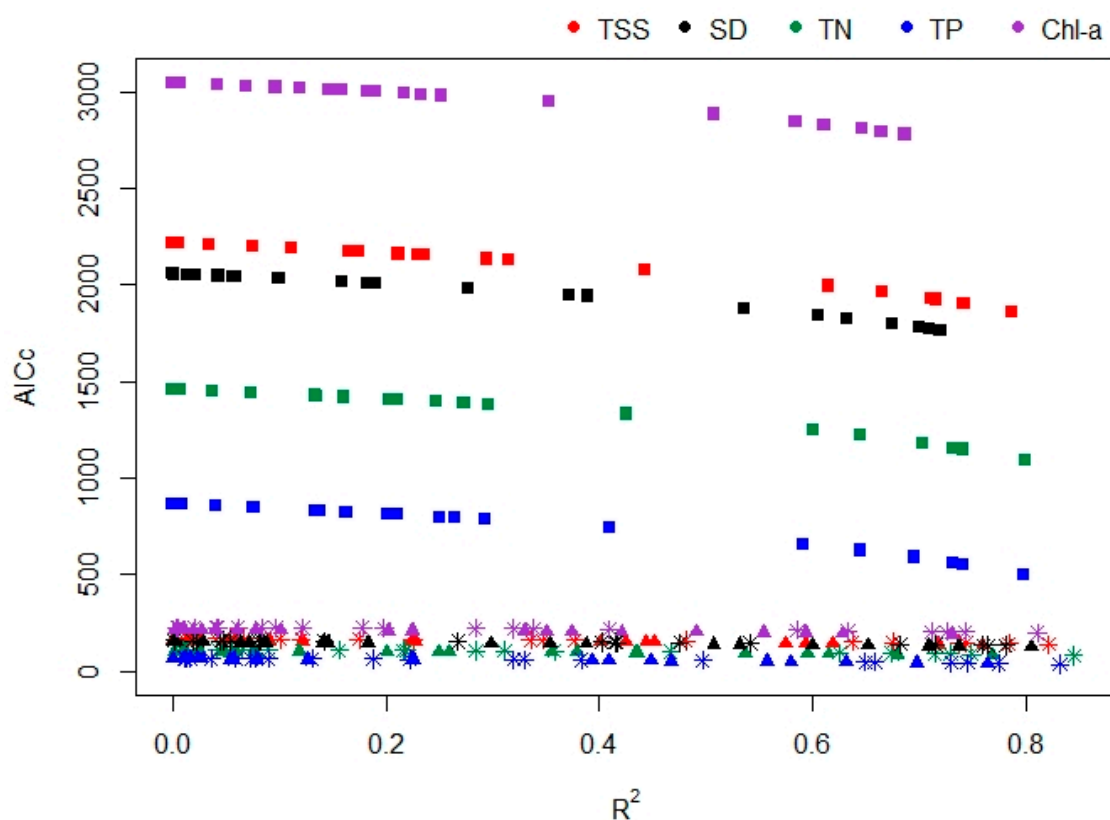


**Figure 10.** Prediction capabilities of all developed models under three extraction scenarios: (1) Point extraction (asterisks), (2) buffer extraction (triangles), and (3) Kriging extraction (squares), using a single variable regression approach.

In order to improve the predictive capabilities of each model developed under the point extraction scenario, a multiple variable linear regression approach was used. Table 4 presents the best performing (highest  $R^2$ ) models for all evaluated water quality parameters, using single and multiple variable linear approaches. From this table, it can be observed that for all water quality parameters, a multiple variable model yielded a higher  $R^2$ . Table 5 presents the estimated statistical coefficients for the multiple linear regression analysis.

**Table 4.** Best predictive water quality models using single and multiple variable linear approaches. WQP refers to the specific water quality parameter, while m and b are estimated coefficients fitting the regression analysis.

WQP	Single Variable Model	R <sup>2</sup>	Multiple Variable Model	R <sup>2</sup>
SDD	=m*(Green) + b	0.781	=m*(Blue/Red) - m*(Green/Red) + m*(Green/Blue) - b	0.888
TSS	=m*(Green/Red) - b	0.821	=m*(Blue/Red) - m*(Green/Red) + m*(Green/Blue) + b	0.987
TN	=m*(Green/Red) - b	0.845	=m*(Blue/Red) - m*(Green/Red) - m*(Green/Blue) + b	0.979
TP	=m*(Green/Red) - b	0.832	=m*(Blue/Red) - m*(Green/Red) + m*(Green/Blue) + b	0.984
Chl-a	=m*(Green/Red) - b	0.810	=m*(Green) - m*(Red) + b	0.846

**Table 5.** Estimated coefficients multiple analysis regression.

WQP	Blue	Green	Green	Green	Red	y-Intercept (b)
	Red	Red	Blue			
Slope (m)						
SDD	164.32	108.33	78.67	-	-	61.91
TSS	264.5	148.2	185.2	-	-	215.3
TN	45.43	26.16	32.94	-	-	36.92
TP	12.441	6.993	8.810	-	-	9.953
Chl-a	-	-	-	9158.79	13,359	27.99

### 3.4. Validation and Spatial Distribution Maps

The developed models and their respective equations were validated using the remaining 50% of the data. Using this validation dataset as input for the models (Table 3), calculated water quality values were generated and compared against the actual in-situ measurements. Given that the R<sup>2</sup> values calculated for each selected model were so close to unity, bias and scatter—both of which evaluate the difference between the predicted values of the model and the real value to be predicted—were very small.

Figure 11 presents a comparison between the actual and predicted optical and non-optical water quality parameters. Further evaluation of the calculated water quality data indicates that the distribution of created data followed a normal distribution (Shapiro-Wilk test *p*-value > 0.05 for all parameters) and that statistically there was no difference between the calculated values and the collected in-situ values (*t*-test *p*-value > 0.05 for all parameters).

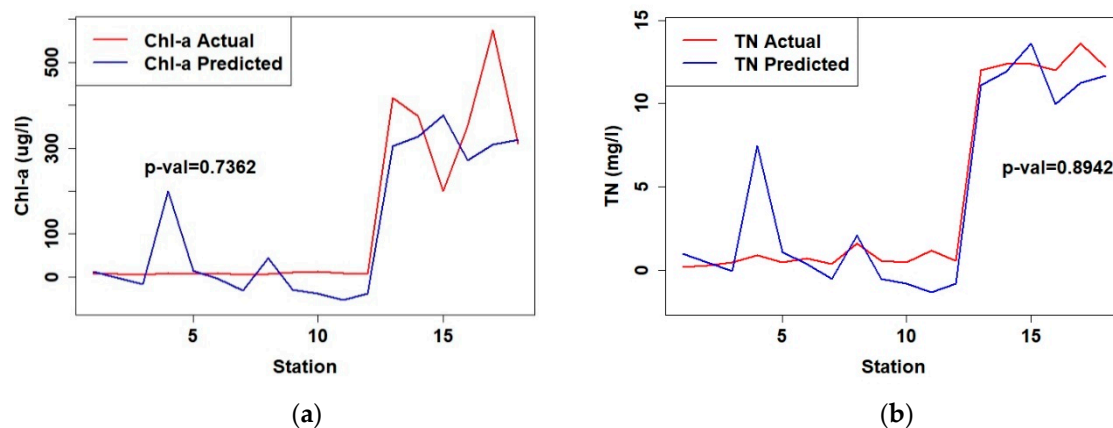


**Figure 11.** Cont.

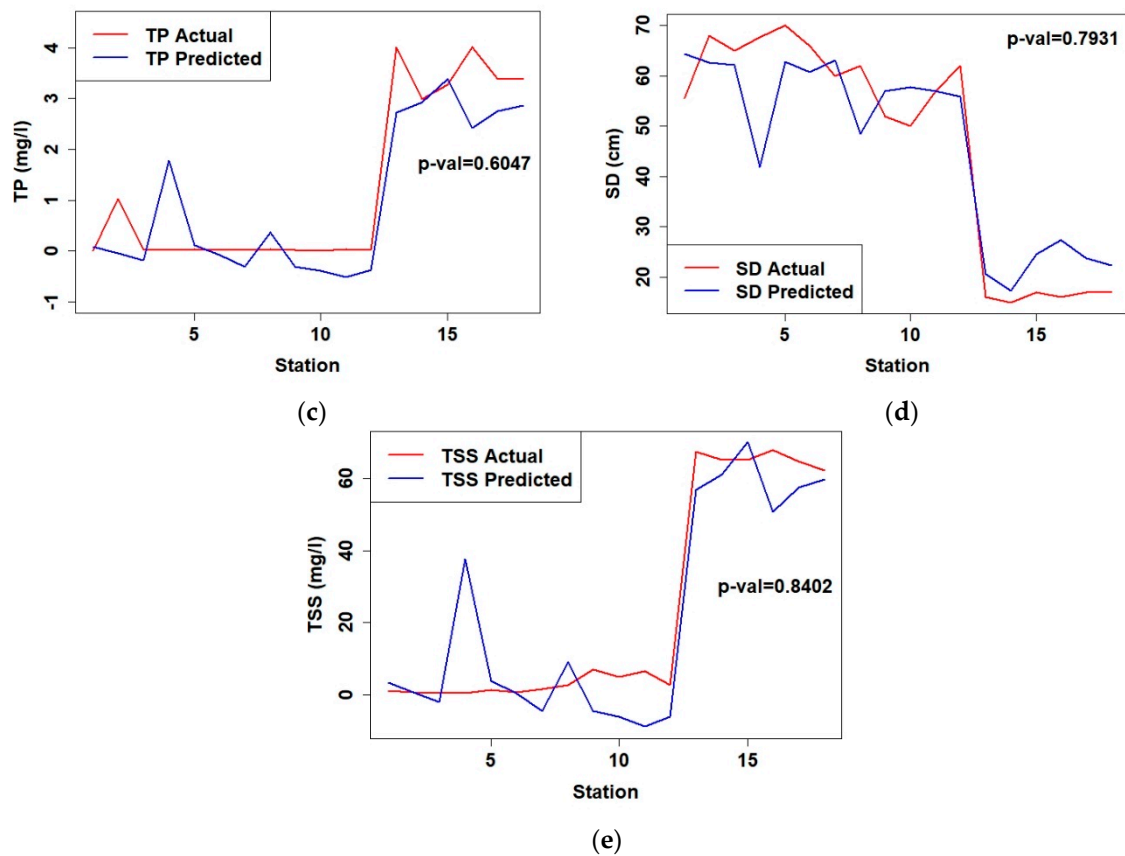


**Figure 11.** Multiple variable models’ comparisons of the actual and predicted optical and non-optical water quality parameters. (a) Chlorophyll-a, (b) total nitrogen, (c) total phosphorous, (d) Secchi disk depth, and (e) total suspended solids.

Once it was determined that there was no statistical difference between the calculated values and the collected in-situ values, band arithmetic function (following the models’ equations) was applied to the collected multispectral images in order to establish spatial distribution maps for all of the water quality parameters in the oligotrophic (Figure 12) and eutrophic (Figure 13) systems.

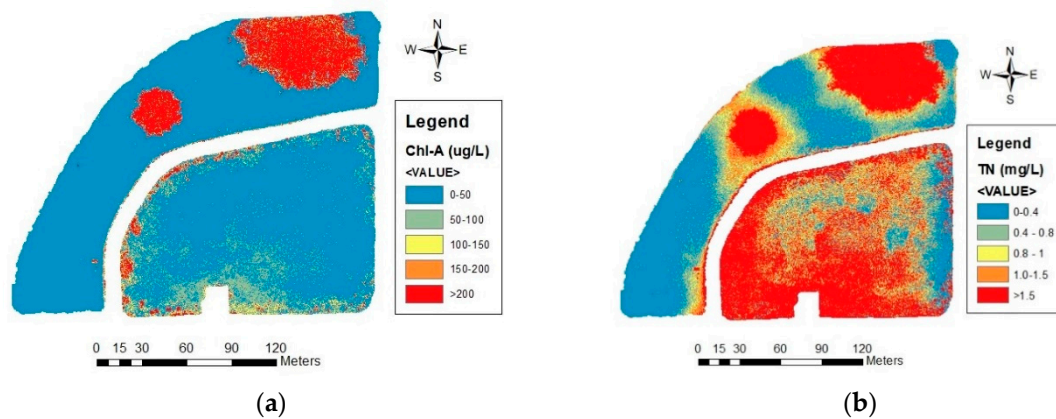


**Figure 12.** Cont.

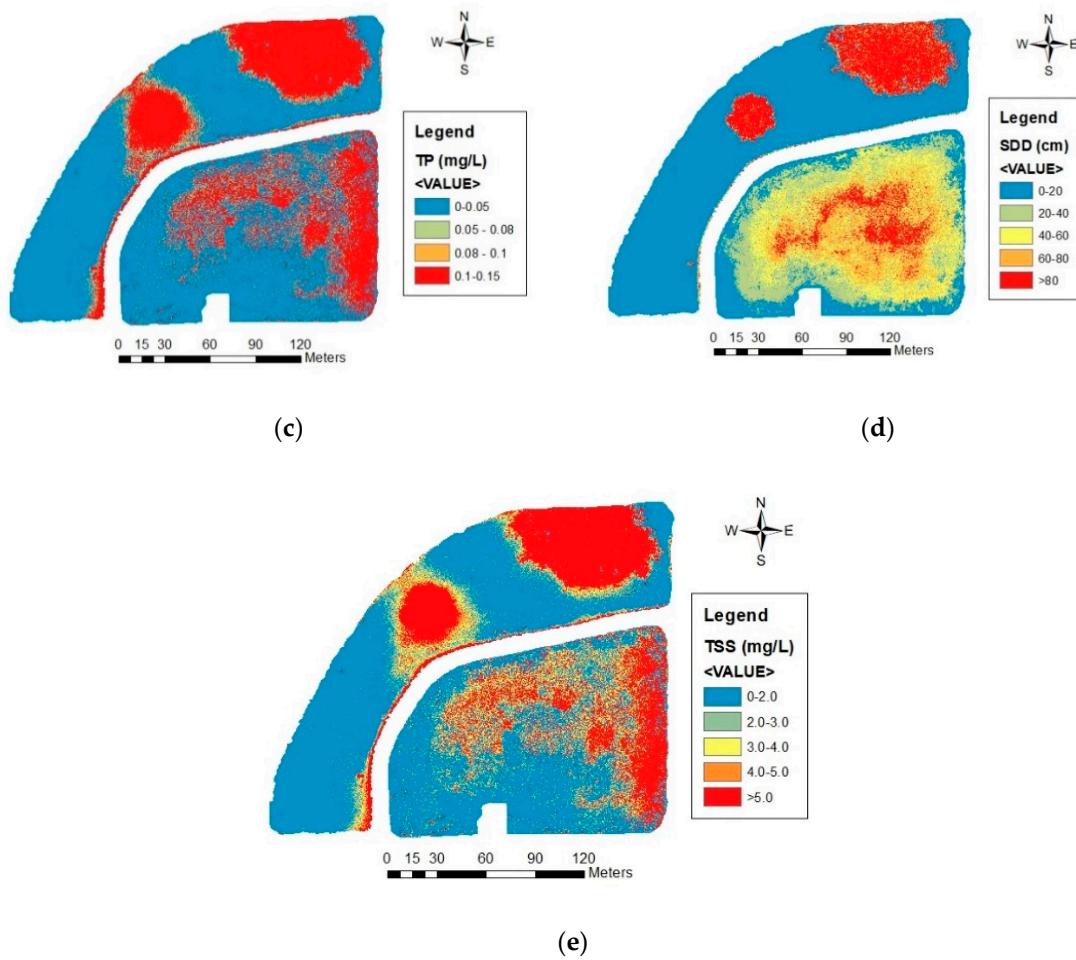


**Figure 12.** Spatial distribution maps for the estimated water quality parameters in the oligotrophic system. (a) Chlorophyll-a, (b) total nitrogen, (c) total phosphorous, (d) Secchi disk depth, and (e) total suspended solids.

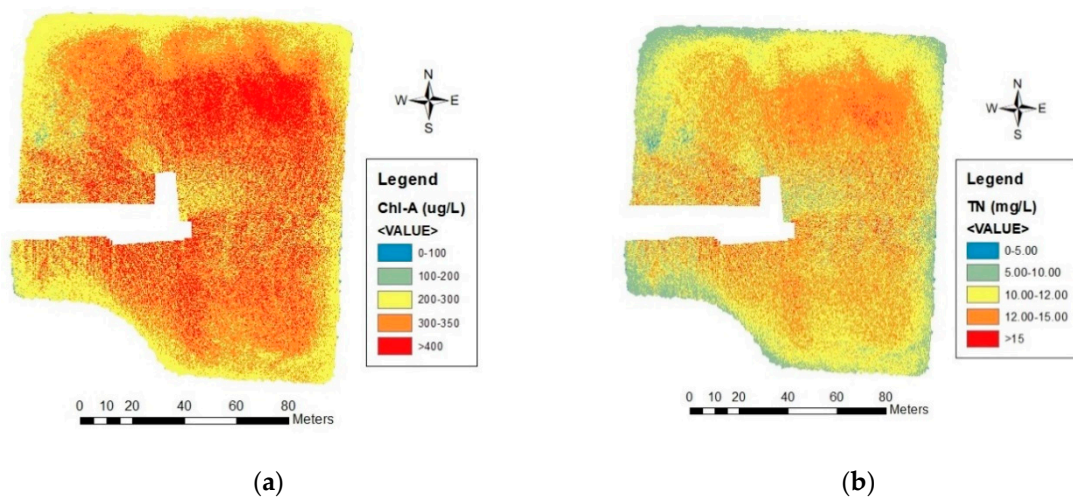


**Figure 13.** Cont.

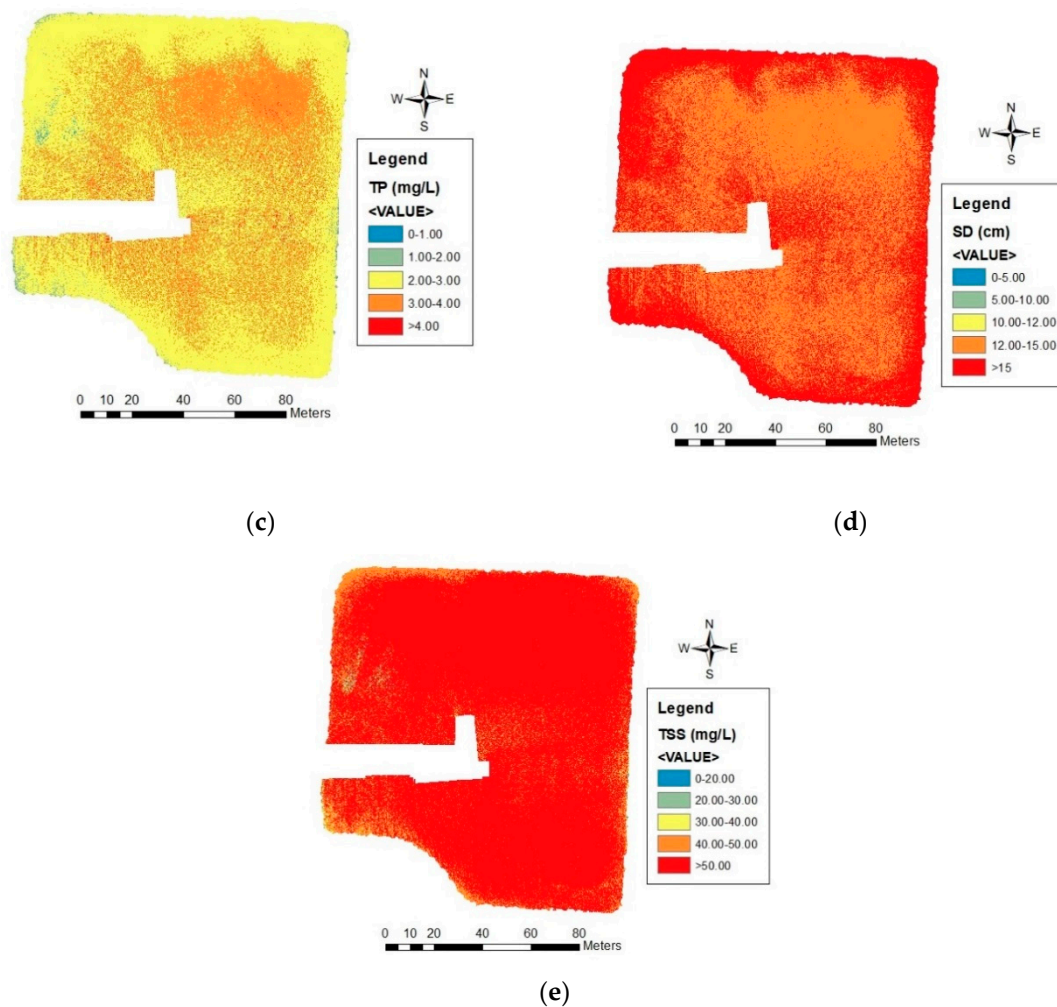


**Figure 13.** Spatial distribution maps for the estimated water quality parameters in the eutrophic system. (a) Chlorophyll-a, (b) total nitrogen, (c) total phosphorous, (d) Secchi disk depth, and (e) total suspended solids. Whited-out sections are due to the inability of the pre-processing software to properly stitch images at those locations.

From the generated spatial distribution maps, it can be observed that both systems (oligotrophic and eutrophic) present fully mixed waters (which correlates to the water quality analyses presented in Section 3.1). Also, it is important to note from the distribution maps for the oligotrophic system, that aquatic features present during the image capturing process (aquatic vegetation, located at north and northeast portion of pond) can be clearly identified from the different optical water quality measurements. At the same time, from Figure 13, it can be observed that that in all distribution maps, there are whited-out sections. These sections are due to the inability of the pre-processing software to properly stitch images at those locations.

#### 4. Discussion

The main purpose of this study was to develop models capable of reliably estimating optical (TSS, Chl-a, and SDD) and non-optical (TP and TN) water quality parameters in two extremes of the aquatic biological productivity spectrum (oligotrophic and eutrophic systems), using in situ data and images collected with a multispectral sensor attached to an sUAS. In order to develop these algorithms, linear approaches using single and multiple variables were used. As a result, it was determined that linear models using multiple variables had stronger predictive capabilities for all water quality parameters.

These algorithms have the capability of generating data that are not statistically different from the collected in-situ data for optical and non-optical water quality parameters.

In the paper “Comprehensive Review on Water Quality Parameters Estimation Using Remote Sensing Techniques”, Gholizabeh et al. [52] references that different authors determined that the use of visible and near infrared bands of the EM spectrum from multispectral sensors can be used to obtain strong correlations between reflectance and optical water quality parameters. However, when exploring correlations for non-optical parameters, direct inference of these measurements had low predictive capabilities. Lim and Choi [53] used Landsat 8 in order to correlate spectral bands with in-situ water quality measurements, in order to establish water quality models capable of estimating optical (TSS and Chl-a) and non-optical (TN and TP) parameters in the Nakdong River in Korea. As a result, they obtained algorithms that strongly estimated TSS and Chl-a ( $R^2 = 0.74$  and  $0.71$ , respectively), but were not as strong when estimating TP and TN ( $R^2 = 0.50$  and  $0.48$ , respectively). Due to this limitation, an indirect estimation approach has been taken by some authors in order to develop strong correlations that relate TP and TN to Chl-a concentrations and SDD [54,55].

When examining the multiple variable models determined by this study (Table 3), it can be observed that the combination between the ratios Blue/Red, Green/Red, and Green/Blue provide the strongest correlation between reflectance and most of the optical and non-optical water quality parameters (except for Chl-a, for which the highest correlation was obtained with the Green and Red bands). These findings are in accordance with Gholizabeh et al. [52]; however, it was determined by this study that these ratios not only have the capability of estimating optical parameters, but also non-optical values. Lui et al. [56] determined that with the use of high-resolution imagery, linear (multiple linear regression) and non-linear (artificial neural network) models with strong predictive capabilities could be developed for TN and TP. The basis of these relationships is explained by the high spectral correlation that TN and TP have with SDD, TSS, and Chl-a [57].

It is imperative to begin this discussion with this information because the study presented herein deviates from the traditional approach of using multispectral sensors attached to satellite platforms. Instead, this study uses a more compact multispectral sensor, attached to an sUAS. By doing this, not only can direct methods of estimating non-optical water quality parameters be derived, but the use of this tool enhances spatial and temporal resolutions while eliminating the cloud coverage issues.

Earth observation satellites are the most common platforms to monitor and collect information about the Earth [58]. Table 6 presents some of the most common remote sensing satellites used for estimating water quality parameters, along with their respective spatial and temporal resolutions. From this table, it can be determined that the spatial resolution obtained by any of these platforms is much coarser when compared to the spatial resolution (6–8 cm) obtained with the sensor used in this study. To illustrate this concept, Figure 14 presents a visual comparison between images taken from two commonly used remote sensing satellites (Landsat 8 and Sentinel-2A) versus the images captured by the sUAS in the eutrophic system used in this study. By looking at these aerial images, the pixel resolution significantly increases in the picture taken with the sUAS.

**Table 6.** Spatial and temporal resolutions of some of the most commonly used remote sensing satellites for water quality estimation, compared to the sUAS used in this study.

Satellite	Spatial Resolution	Temporal Resolution (Day)
Landsat-5	30 m	16
Landsat-7	30 m	16
Landsat-8	30 m	16
QuickBird-2	15 m	1–3
Orb View-3	4 m	3
Gaofen-1	8 m	4
Sentinel-2	10 m	5
sUAS	0.06–0.08 m	Flight-specific

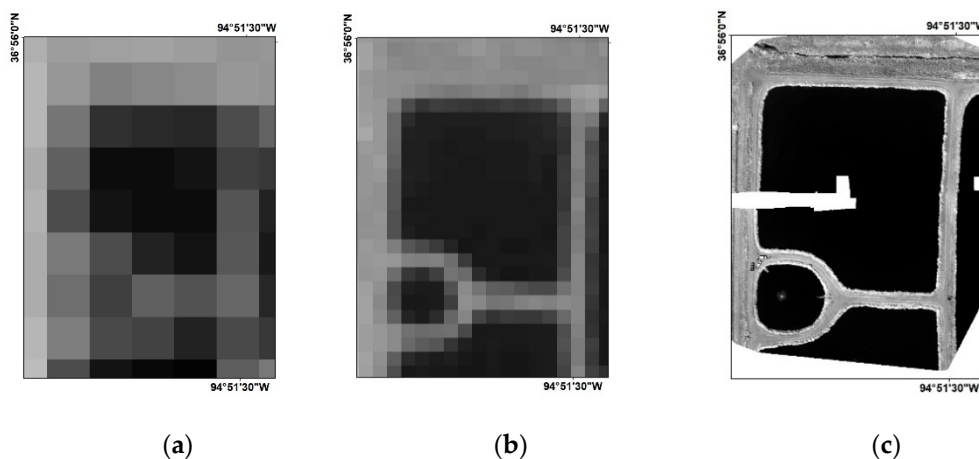


**Figure 14.** Remote sensing imagery collected at the eutrophic system by Landsat-8 (a), Sentinel-2A (b), and sUAS (c).

The use of satellite remote sensing tools helps to expand the limited discrete sampling point coverage of traditional monitoring plans [3,6,26,59,60]. However, in addition to spatial resolution, two major drawbacks when using these tools are: (1) The longer revisiting time (temporal resolution) of these platforms and (2) cloud coverage limitations. Zhang and Kovacs [61] point out that the longer temporal resolutions of some of these platforms presents a major difficulty when trying to monitor systems that are in a constant state of change. At the same time, other authors mention that the number of images that they are unable to use due to cloud coverage accounts in some cases for up to 97% of the available captured imagery for a particular region in a 25-year period [3]. With the use of sUASs, these issues are no longer a concern. First, with an sUAS, the operator has the flexibility of deciding how often they want to capture multispectral imagery. Secondly, because sUAS fly below the clouds, all the imagery is 100% cloud coverage free.

In order to determine optical and non-optical water quality measurements from multispectral sensors, in-situ measurements are needed to develop and calibrate the different models [26]. However, due to the above limitations for use of satellite imagery, selecting images for these types of correlations can become a non-trivial task. Hicks et al. [62] suggest that ideal imagery for these types of studies should not be more than one day apart from the in-situ data collection. However, in most cases, this is not possible due to the temporal resolution of the platform or cloud coverage present in the imagery [3,6,26,60,61]. Furthermore, Barrett and Frazier [63] mention that water quality parameters can be directly influenced by rapidly changing environmental conditions in the study site, and as a result, the utility of predictive models developed from imagery that is generated days or weeks from the day of the in-situ sampling can be detrimentally impacted. As shown in Table 1, with the use of an sUAS, the time window between water sample acquisition and multispectral imagery collection can be reduced to minutes to hours. In theory, and due to the flexibility that these portable platforms provide, decreasing the time window between water sample acquisition and multispectral imagery collection translates to stronger and more reliable water quality models.

A secondary objective of this study was to evaluate if using a statistical interpolation method improved the algorithms between the different optical and non-optical water quality parameters and the reflectance values. In order to do that, three scenarios were evaluated under the reflectance extraction procedures: (1) Point extraction, (2) buffer extraction, and (3) kriging extraction. Results indicated that models created from the first scenario (point extraction) presented stronger predictive capabilities. Mu et al. [64] references that in spatial sampling, collected samples are not independent from each other and for that reason the number of samples that need to be taken in order to develop or validate remote sensing products can be decreased in order to improve accuracy. Considering the water quality results and the spatial distribution maps generated in this study, it makes sense that

for fully mixed systems (such as the ponds used in this study), fewer sample stations led to more accurate models.

For all the points discussed, one can determine that the use of sUAS offers additional benefits than the traditional satellite remote sensing approach. However, it is important to point out that sUAS, just like any other remote sensing tool, have their limitations. The first and perhaps the most important limiting factor when using this technology is the weather. When planning missions with sUAS, the operator must be aware that these platforms are unable to fly under wet conditions (rain) and elevated wind speeds (higher than 5 m/s or as stipulated by the platform manufacturer). For the study presented above, these issues were not a concern. However, it is necessary to point this out, because even though sUAS offer more advantages when it comes to obtaining imagery capable of estimating optical and non-optical water quality parameters, there is a tradeoff that needs to be considered and evaluated by the user.

## 5. Conclusions

This study aimed to create different statistical water quality models for optical (TSS, SDD, and Chl-a) and non-optical (TP and TN) water quality parameters in oligotrophic and eutrophic aquatic systems using remote sensing images from an sUAS equipped with a multispectral sensor. From the results of this study, it can be concluded that: (1) When using a multiple linear regression approach, models capable of predicting optical and non-optical models (with strong prediction capability  $R^2 > 0.80$ ) can be created, (2) multiple variable linear regressions in the visible portion of the electromagnetic spectrum (blue, green, and red) best described the relationship between TSS ( $R^2 = 0.99$ ,  $p$ -value =  $<0.01$ ), Chl-a ( $R^2 = 0.85$ ,  $p$ -value =  $<0.01$ ), TP ( $R^2 = 0.98$ ,  $p$ -value =  $<0.01$ ), TN ( $R^2 = 0.98$ ,  $p$ -value =  $<0.01$ ), and SDD ( $R^2 = 0.88$ ,  $p$ -value =  $<0.01$ ), (3) the use of statistical interpolation (ordinary kriging) does not improve the statistical relationship between the different water quality parameters and the reflectance values, (4) 100% cloud free imagery can be collected with the use of sUAS, (5) the use of sUAS for water quality monitoring allows the user more flexibility in terms of temporal and spatial resolution, and (6) future research should evaluate if the use of this technology improves the predictive capabilities of water quality models that rely on satellite imagery and if the models developed in this study have the capacity of determining water quality in reservoirs that fall in other portions of the biological productivity spectrum.

**Author Contributions:** Conceptualization, J.G.A. and R.W.N.; methodology, J.G.A. and R.W.N.; validation, J.G.A. and R.W.N.; formal analysis, J.G.A. and R.W.N.; investigation, J.G.A. and R.W.N.; resources, R.W.N.; writing—original draft preparation, J.G.A.; writing—review and editing, R.W.N.; visualization, R.W.N.; supervision, R.W.N.; project administration, R.W.N.; funding acquisition, R.W.N. All authors have read and agreed to the published version of the manuscript.

**Funding:** This research was funded by the Grand River Dam Authority (GRDA), grant numbers 100052 and A15-0240.

**Acknowledgments:** The authors would like to acknowledge the Grand River Dam Authority (GRDA) Ecosystems and Education Center (EEC) for providing financial support and invaluable assistance to make this project possible, and the City of Commerce for site access. Special thanks are given to Darrell Townsend, Steve Nikolai, Dustin Browning and Matthew Conrad at GRDA EEC. Field and laboratory assistance provided by members of the Center for Restoration of Ecosystems and Watersheds (CREW) at the University of Oklahoma is gratefully acknowledged.

**Conflicts of Interest:** The authors declare no conflict of interest.

## References

1. United States Geological Survey. Measuring and Monitoring Water. Available online: <https://www.usgs.gov/mission-areas/water-resources/science/measuring-and-monitoring-water> (accessed on 10 December 2019).
2. Wilde, F.D. Field Measurements: U.S. Geological Survey Techniques of Water-Resources Investigations. Available online: <http://pubs.water.usgs.gov/twri9A6/> (accessed on 10 December 2019).
3. Kloiber, S.M.; Brezonik, P.L.; Olmanson, L.G.; Bauer, M.V. A procedure for regional lake water clarity assessment using landsat multispectral data. *Remote Sens. Environ.* **2002**, *82*, 38–47. [CrossRef]

4. Zhao, D.; Cai, Y.; Jiang, H.; Xu, D.; Zhang, W.; An, S. Estimation of water clarity in taihu lake and surrounding rivers using landsat imagery. *Adv. Water Resour.* **2011**, *34*, 165–173. [[CrossRef](#)]
5. Ritchie, J.C.; Zimba, P.V.; Everitt, J.H. Remote sensing techniques to assess water quality. *Am. Soc. Photogramm. Remote Sens.* **2003**, *6*, 695–704. [[CrossRef](#)]
6. Olmanson, L.G.; Bauer, M.E.; Brezonik, P.L. A 20-year landsat water clarity census of minnesota's 10,000 lakes. *Remote Sens. Environ.* **2008**, *112*, 4086–4097. [[CrossRef](#)]
7. Brezonik, P.L.; Olmanson, L.G.; Finlay, J.C.; Bauer, M.E. Factors affecting the measurement of CDOM by remote sensing of optically complex inland waters. *Remote Sens. Environ.* **2015**, *157*, 199–215. [[CrossRef](#)]
8. Baban, S.J. Detecting water quality parameters in the norfolk broads, U.K., using landsat imagery. *Int. J. Remote Sens.* **2007**, *14*, 1247–1267. [[CrossRef](#)]
9. Dominguez, J.A.; Chuvieco, E.; Sastre-Merlin, A. Monitoring transparency in inland water bodies using multispectral images. *Int. J. Remote Sens.* **2009**, *30*, 1567–1586. [[CrossRef](#)]
10. Duan, H.; Ma, R.; Hu, C. Evaluation of remote sensing algorithms for cyanobacterial pigment retrievals during spring bloom formation in several lakes of east China. *Remote Sens. Environ.* **2012**, *126*, 126–135. [[CrossRef](#)]
11. Matthews, M.W.; Bernard, S.; Robertson, L. An algorithm for detecting trophic status (chlorophyll-a), cyanobacterial-dominance, surface scums and floating vegetation in inland and coastal waters. *Remote Sens. Environ.* **2012**, *124*, 637–652. [[CrossRef](#)]
12. Ma, J.; Qin, B.; Wu, P.; Zhou, J.; Niu, C.; Deng, J.; Niu, H. Controlling cyanobacteria blooms by managing nutrient ratio and limitation in large hyper-eutrophic lake: Lake Taihu, China. *J. Environ. Sci.* **2015**, *27*, 80–86. [[CrossRef](#)]
13. Mobley, C.; Stramski, D.; Bissett, W.; Boss, E. Optical modeling of ocean waters: Is the Case 1–Case 2 classification still useful? *Oceanography* **2004**, *17*, 60–67. [[CrossRef](#)]
14. Morel, A.; Belanger, S. Improved detection of turbid waters from ocean color sensors information. *Remote Sens. Environ.* **2006**, *102*, 237–249. [[CrossRef](#)]
15. Forget, P.; Ouillon, S.; Lahet, F.; Broche, P. Inversion of reflectance spectra of nonchlorophyllous turbid coastal waters. *Remote Sens. Environ.* **1999**, *68*, 264–272. [[CrossRef](#)]
16. Lee, Z.; Hu, C. Global distribution of Case-1 waters: An analysis from seawifs measurements. *Remote Sens. Environ.* **2006**, *101*, 270–276. [[CrossRef](#)]
17. Kirk, J.T.O. Optical water quality—What does it mean and how should we measure it? *J. Water Pollut. Control Fed.* **1988**, *60*, 194–197.
18. International Ocean-Colour Coordinating Group (IOCCG). *Why the Ocean Color? The Societal Benefits of Ocean-Colour Technology*; International Ocean Colour Coordinating Group (IOCCG): Dartmouth, NS, Canada, 2008; p. 141.
19. International Ocean-Colour Coordinating Group (Ioccg). *Earth Observations in Support of Global Water Quality Monitoring*; International Ocean Colour Coordinating Group (IOCCG): Dartmouth, NS, Canada, 2018; p. 132.
20. Lillesand, T.M.; Johnson, W.L.; Deuell, R.L.; Lindstrom, O.M.; Meisner, D.E. Use of landsat data to predict the trophic state of minnesota lakes. *Photogramm. Eng. Remote Sens.* **1983**, *49*, 219–229.
21. Giardino, C.; Pepe, M.; Brivio, P.A.; Ghezzi, P.; Zilioli, E. Detecting chlorophyll, secchi disk depth and surface temperature in a sub-alpine lake using landsat imagery. *Sci. Total. Environ.* **2001**, *268*, 19–29. [[CrossRef](#)]
22. Asner, G.P. Cloud cover in landsat observations of the brazilian amazon. *Int. J. Remote Sens.* **2010**, *22*, 3855–3862. [[CrossRef](#)]
23. Nelson, S.; Soranno, P.A.; Spence Cheruvilil, K.; Batzli, S.; Skole, D.L. Regional assessment of lake water clarity using satellite remote sensing. *Educ. J. Limnol.* **2003**, *32*, 27–32. [[CrossRef](#)]
24. Torbick, N.; Hu, F.; Zhang, J.; Qi, J.; Zhang, H.; Becker, B. Mapping chlorophyll-a concentrations in west lake, China using landsat 7 ETM+. *J. Great Lakes Res.* **2008**, *34*, 559–565. [[CrossRef](#)]
25. Guan, X.; Li, J.; Booty, W.G. Monitoring lake simcoe water clarity using landsat-5 TM images. *Water Resour. Manag.* **2011**, *25*, 2015–2033. [[CrossRef](#)]
26. Bonansea, M.; Rodriguez, M.C.; Pinotti, L.; Ferrero, S. Using multi-temporal landsat imagery and linear mixed models for assessing water quality parameters in río tercero reservoir (argentina). *Remote Sens. Environ.* **2015**, *158*, 28–41. [[CrossRef](#)]
27. Colomina, I.; Molina, P. Unmanned aerial systems for photogrammetry and remote sensing: A review. *ISPRS J. Photogramm. Remote Sens.* **2014**, *92*, 79–97. [[CrossRef](#)]

28. Rusnak, M.; Sladek, J.; Kidova, A.; Lehotsky, M. Template for high-resolution river landscape mapping using UAV technology. *Measurement* **2018**, *115*, 139–151. [CrossRef]
29. Louhaichi, M.; Petersen, S.; Gomez, T.; Jensen, R.R.; Morgan, G.R.; Butterfield, C. Remote spectral imaging using a low cost sUAV system for monitoring rangelands. *Adv. Remote Sens. Geo Inform. Appl.* **2018**, *1*, 143–145. [CrossRef]
30. Doughty, C.; Cavanaugh, K. Mapping coastal wetlands biomass from high resolution unmanned aerial vehicle (UAV) imagery. *Remote Sens.* **2019**, *11*, 540. [CrossRef]
31. Melville, B.; Fisher, A.; Lucieer, A. Ultra-high spatial resolution fractional vegetation cover from unmanned aerial multispectral imagery. *Int. J. Appl. Earth Obs. Geoinf.* **2019**, *78*, 14–24. [CrossRef]
32. Berni, J.A.; Zarco-Tejada, P.J.; Suarez, L.; Fereres, E. Thermal and narrowband multispectral remote sensing for vegetation monitoring from an unmanned aerial vehicle. *IEEE Trans. Geosci. Remote Sens.* **2009**, *47*, 722–738. [CrossRef]
33. Nebiker, S.; Lack, N.; Abacherli, M. Light-weight multispectral UAV sensors and their capabilities for predicting grain yield and detecting plant diseases. *Int. Arch. Photogramm. Remote Sens. Spat. Inf. Sci.* **2016**, *XLI-B1*, 963–970. [CrossRef]
34. Su, T.; Chou, H. Application of multispectral sensors carried on unmanned aerial vehicle (UAV) to trophic state mapping of small reservoirs: A case study of tain-pu reservoir in Kinmen, Taiwan. *Remote Sens.* **2015**, *7*, 10078–10097. [CrossRef]
35. Kageyama, Y.; Takahashi, J.; Nishida, M.; Kobori, B.; Nagamoto, D. Analysis of water quality in Miharu dam reservoir, Japan, using UAV data. *IEEE Trans. Electr. Electron. Eng. Jpn.* **2016**, *11*, 183–185. [CrossRef]
36. Anderson, C.R.; Berdalet, E.; Kudela, R.M.; Cusack, C.K.; Silke, J.; O'Rourke, E.; Dugan, D.; McCammon, M.; Newton, J.A.; Moore, S.K.; et al. Scaling up from regional case studies to a global harmful algal bloom observing system. *Front. Mar. Sci.* **2019**, *6*. [CrossRef]
37. Schmale, D.G.; Ault, A.P.; Saad, W.; Scott, D.T.; Westrick, J.A. Perspectives on harmful algal blooms (HABs) and the cyberbiosecurity of freshwater systems. *Front. Bioeng. Biotechnol.* **2019**, *7*. [CrossRef] [PubMed]
38. Carlson, R.E. A trophic state index for lakes. *Limnol. Oceanogr.* **1977**, *22*, 361–369. [CrossRef]
39. Davis, T.W.; Stumpf, R.; Bullerjahn, G.S.; McKay, R.M.; Chaffin, J.D.; Bridgeman, T.B.; Winslow, C. Science meets policy: A framework for determining impairment designation criteria for large waterbodies affected by cyanobacterial harmful algal blooms. *Harmful Algae* **2019**, *81*, 59–64. [CrossRef] [PubMed]
40. Mesonet. Local Conditions. Available online: <https://www.mesonet.org/index.php/weather/local> (accessed on 10 December 2019).
41. Oklahoma Department of Environmental Quality. Lagoon Sewage Treatment Systems. Available online: <https://www.deq.ok.gov/wp-content/uploads/environmental-complaints/Lagoon-.pdf> (accessed on 10 December 2019).
42. YSI Incorporated. 6-Series Multiparameter Water Quality Sondes User Manual. Available online: <https://www.ysi.com/File%20Library/Documents/Manuals/069300-YSI-6-Series-Manual-RevJ.pdf> (accessed on 7 December 2019).
43. United States Environmental Protection Agency. *Methods for Chemical Analysis of Waters and Waste Waters*; EPA/600/4-79/020 (NTIS PB84128677); U.S. Environmental Protection Agency: Washington, DC, USA, 2002.
44. Aerial Technology International. ATI AgBOT Data Sheet. Available online: <http://store.aerialtechnology.com/product/agbot-2/> (accessed on 7 December 2019).
45. Mission Planner; Computer Software. ArduPilot Development Team. Available online: <https://ardupilot.org/planner/> (accessed on 23 December 2019).
46. *Pix4Dmapper*; Computer Software; Pix4D SA: Prilly, Switzerland, 2011.
47. *ArcMap*; Computer Software; Environmental Systems Research Institute (ESRI): Redlands, CA, USA, 2012.
48. Akaike, H. Information Theory and an Extension of the Maximum Likelihood Principle. In Proceedings of the 2nd International Symposium on Information Theory, Tsahkadsor, Armenia, 2–8 September 1971; Akadémiai Kiadó: Budapest, Hungary, 1973; pp. 267–281.
49. Burnham, K.P.; Anderson, D.A. *Model Selection and Multimodel Inference*, 2nd ed.; Springer: New York, NY, USA, 2002; pp. 1–488.
50. Shapiro, S.S.; Wilk, M.B. An analysis of variance test for normality (complete samples). *Biometrika* **1965**, *52*, 591–611. [CrossRef]
51. R Core Team. *R Computer Software*; R Core Team: Vienna, Austria, 2017.

52. Gholizadeh, M.H.; Melesse, A.M.; Reddi, L. A comprehensive review on water quality parameters estimation using remote sensing techniques. *Sensors* **2016**, *16*, 1298. [[CrossRef](#)]
53. Lim, J.; Choi, M. Assessment of water quality based on landsat 8 operational land imager associated with human activities in Korea. *Environ. Monit. Assess.* **2015**, *187*, 384–401. [[CrossRef](#)]
54. Wu, C.; Wu, J.; Qi, J.; Zhang, L.; Huang, H.; Lou, L.; Chen, Y. Empirical estimation of total phosphorus concentration in the mainstream of the qiantang river in China using landsat TM data. *Int. J. Remote Sens.* **2010**, *31*, 2309–2324. [[CrossRef](#)]
55. Sharaf El Din, E.; Zhang, Y. Estimation of both optical and non-optical surface water quality parameters using landsat 8 OLI imagery and statistical techniques. *J. Appl. Remote Sens.* **2017**, *11*, 046008. [[CrossRef](#)]
56. Liu, J.; Zhang, Y.; Yuan, D.; Song, X. Empirical estimation of total nitrogen and total phosphorus concentration of urban water bodies in China using high resolution IKONOS multispectral imagery. *Water* **2015**, *7*, 6551–6573. [[CrossRef](#)]
57. Song, K.; Li, L.; Li, S.; Tedesco, L.; Hall, B.; Li, L. Hyperspectral remote sensing of total phosphorus (TP) in three central indian water supply reservoirs. *Water Air Soil Pollut.* **2012**, *223*, 1481–1502. [[CrossRef](#)]
58. Liu, X.; Chen, Y.; Chen, Y.; He, R. Optimization of earth observation satellite system based on parallel systems and computational experiments. *J. Control Theory Appl.* **2013**, *11*, 200–206. [[CrossRef](#)]
59. Allan, M.G.; Hamilton, D.P.; Hicks, B.J.; Brabyn, L. Landsat remote sensing of chlorophyll-a concentrations in central north island lakes of New Zealand. *Int. J. Remote Sens.* **2011**, *32*, 2037–2055. [[CrossRef](#)]
60. Mushtaq, F.; Nee Lala, M.G. Remote estimation of water quality parameters of himalayan lake (kashmir) using landsat 8 OLI imagery. *Geocarto Int.* **2017**, *32*, 274–285. [[CrossRef](#)]
61. Zhang, C.; Kovacs, J.M. The application of small unmanned aerial systems for precision agriculture: A review. *Precis. Agric.* **2012**, *12*, 693–712. [[CrossRef](#)]
62. Hicks, B.J.; Stichbury, G.A.; Brabyn, L.K.; Allan, M.G.; Ashraf, S. Hindcasting water clarity from landsat satellite images of unmonitored shallow lakes in the Waikato Region, New Zealand. *Environ. Monit. Assess.* **2013**, *185*, 7245–7261. [[CrossRef](#)]
63. Barrett, D.C.; Frazier, A.E. Automated method for monitoring water quality using landsat imagery. *Water* **2016**, *8*, 257. [[CrossRef](#)]
64. Mu, X.; Hu, M.; Song, W.; Ruan, G.; Ge, Y.; Wang, J.; Huang, S.; Yan, G. Evaluation of sampling methods for validation of remotely sensed fractional vegetation cover. *Remote Sens.* **2015**, *7*, 16164–16182. [[CrossRef](#)]



© 2019 by the authors. Licensee MDPI, Basel, Switzerland. This article is an open access article distributed under the terms and conditions of the Creative Commons Attribution (CC BY) license (<http://creativecommons.org/licenses/by/4.0/>).